

## Letters

Near-Field Surface Plasmon Excitation  
on Structured Gold FilmsBogdan Dragnea,<sup>\*,†</sup> Jodi M. Szarko,<sup>‡</sup> Stefan Kowarik,<sup>§</sup> Thomas Weimann,<sup>#</sup>  
Jochen Feldmann,<sup>§</sup> and Stephen R. Leone<sup>‡</sup>

*Department of Chemistry, Indiana University, Bloomington, Indiana 47405-7102,  
Departments of Chemistry and Physics and Lawrence Berkeley National, Laboratory,  
University of California, Berkeley, California 94720, Sektion Physik and  
Center for Nanoscience, Lehrstuhl für Photonik und Optoelektronik,  
Amalienstr. 54 D-80799 München, Germany, and Physikalisch Technische  
Bundesanstalt, Bundesallee 100, 38116 Braunschweig, Germany*

*Received June 18, 2002; Revised Manuscript Received September 17, 2002*

## ABSTRACT

Surface plasmon polariton (SPP) localization control on rough metal surfaces has been achieved by varying the gap between a scanning near-field aperture probe and the surface. The qualitative explanation for this observation is based on the overlapping of spatial frequencies available for near-field excitation of the SPP, with the spectral distribution of spatial frequencies characterizing the surface roughness. From a practical point of view, this selective excitation of electromagnetic states on nanostructures provides a way to estimate the reflectivity of structures such as grooves engraved into the metal film. Qualitative aspects of transmission and scattering through parallel slit pairs acting as Fabry–Perot resonators are discussed.

Surface plasmon polaritons (SPPs) are collective electron density fluctuations coupled to an outer electromagnetic field which propagate at a metal surface and decay exponentially along the normal to the surface.<sup>1</sup> They have been extensively studied in the past in relation to the field enhancement effect involved in nonlinear surface processes such as surface enhanced Raman scattering,<sup>2</sup> the fluorescence quenching of molecular dyes in the vicinity of metal surfaces,<sup>3,4</sup> and the shape resonance of metal nanoparticles.<sup>5</sup>

More recently, special attention has been given to the interaction between SPPs and nanostructures,<sup>6,7</sup> due to its importance in practical problems relevant to microanalytical sensor integration,<sup>8,9</sup> microelectronics,<sup>10</sup> photonics,<sup>11</sup> and structural rational design of SERS substrates.<sup>12</sup> Experimental investigations with sub-wavelength spatial resolution have been facilitated by the direct local excitation of SPPs by near-field optical probes.<sup>13–16</sup> It has been demonstrated that with suitable tips one can directly map the predicted electromagnetic eigenmodes associated with nanostructures<sup>17</sup> and that, close to nanostructures, the weighting of the nonradiative eigenmodes exceeds that of the radiative eigenmodes, with the optical local density of states (LDOS) being dominated

\* Corresponding author. E-mail: dragnea@indiana.edu

† Indiana University.

‡ University of California, Berkeley.

§ Lehrstuhl für Photonik und Optoelektronik.

# Physikalisch Technische Bundesanstalt.

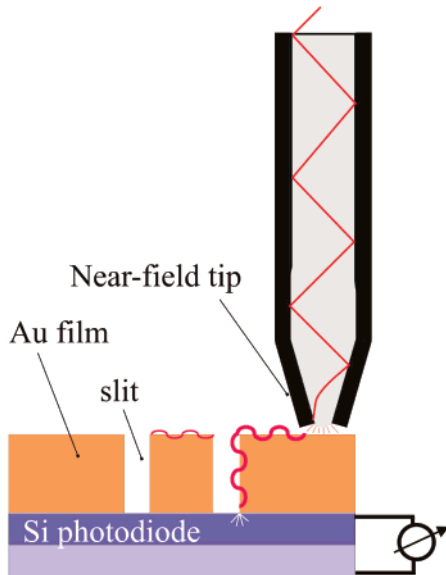


**Figure 1.** Schematic of the photocurrent measurement of surface plasmons excited on a structured metal film by a near-field aperture.

by sub-wavelength features.<sup>18</sup> We show here that using a near-field optical fiber aperture tip, one can selectively excite different spectral regions of the LDOS of a nanostructured, optically thick gold film. To this end, we use the gap between the near-field probe and the nanostructured metal surface as the variable allowing for manipulation of the spectrum of excited electromagnetic eigenmodes of the surface.

The interaction of SPPs in thin silver films with narrow slits using a near-field excitation scheme has been studied by Bouhelier et al.<sup>19</sup> This previous work is different from our approach in two respects. When using our technique, the film can be arbitrarily thick. SPPs at the air/metal surface are decoupled from the buried semiconductor/metal interface. Another difference is that we detect the surface plasmons directly through semiconductor excitations without the need for reconversion to far-field propagating optical radiation. In the second part of the paper, we estimate the reflection coefficient of a slit in an optically thick gold film and we discuss qualitative aspects of transmission and scattering through parallel slit pairs.

The experimental setup is similar to the one described by Sönnichsen et al.,<sup>20</sup> Figure 1. A 250 nm thick gold film is evaporatively deposited onto a photodiode surface. An aluminum-coated, glass fiber, near-field scanning optical microscope tip launches SPPs, which travel along the air/metal surface and hit 150 nm wide, 1.5  $\mu\text{m}$  long slits etched into the film down to the photodiode surface. Then, the SPPs are transferred from the air side of the film to the silica side through the nanoslits connecting the two surfaces and decay into semiconductor excitations detectable as photocurrent. This scheme effectively provides a  $2\pi$  srad detection angle, which offers the advantage of a direct connection between the image and the local density of states.<sup>18</sup> Our setup uses 25 mW of the fundamental and the second harmonic of a Ti:sapphire mode-locked laser, to provide a basis for comparison between plasmon-mediated and direct photon-generated photocurrent in the Si photodiode underlying the

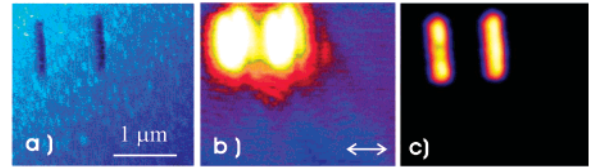


**Figure 2.** (a) Shear-force topographic image, (b) photocurrent image at 775 nm, and (c) photocurrent image at 400 nm excitation wavelength. Images are taken at the same detection sensitivity, which is saturated above the slits in the (b) panel, at 125 nA. Light is partially polarized ( $\sim 70\%$ ) perpendicular to the slit.

gold nanostructured sample. In addition to the deep etched slits, the surface has a statistical roughness characterized by Au dots on a relatively flat surface with an average size of 150 nm  $\times$  10 nm, with a relative lateral size standard deviation of  $\sim 20\%$ .

Photocurrent generated at the slit bottom surface is measured as a function of the tip position on the sample surface. The near-field aperture diameter is 80–100 nm. Far-field measured light polarization emerging from the tip is preserved in a proportion of better than 70% with respect to the coupled light at the fiber input. On optically thick films such as those in this work, the surface plasmons at the air/gold and silica/gold surfaces do not couple, as in other near-field experiments, and there is no light transmitted through the film, either. It follows that the only possibility for semiconductor excitations to occur when the tip is away from the slit, is by nonradiative local fields, i.e., SPPs propagating between the tip and the nanoslits. Figure 2 shows this effect: at 400 nm excitation wavelength, SPPs do not propagate over detectable distances due to the strong absorption in Au at this wavelength. A photocurrent is therefore generated in this case only by direct absorption of photons when the tip is located just above the slit. When changing the wavelength to 775 nm, a signal is present for every location of the tip on the surface. The spatial scale involved in the differences between the photocurrent maps of Figure 2 is too large to be an artifact due to the differences in resolution of near-field tips at different wavelengths.<sup>21–22</sup> Moreover, we routinely check our tips by comparing the far-field diffracted light from the tip with the theoretical Airy distribution at 400 and 775 nm. Only the tips showing good agreement with the theoretical diffraction pattern are used.

The presence of a signal throughout the entire scanned area is therefore the result of the SPP excitation, which transfers the electromagnetic energy from the tip to the semiconductor surface on the bottom of the nanoslits. For the same photon density coupled at the fiber input, the absolute maximum of the photocurrent intensity at 775 nm is 2–3 times larger than at 400 nm. According to the Bethe–Bouwkamp approximation,<sup>23</sup> the transmitted light should vary as  $(a/\lambda)^4$ , where  $a$  is the aperture diameter. Therefore, at 775 nm the photon flux is  $\sim 15$  times smaller than at 400 nm. However, the Bethe–Bouwkamp approximation does not take into account the fiber losses, which in our case are 10 times larger at 400 nm than at 775 nm. Taking into account all these factors, we infer that SPP-assisted coupling through a single slit is 3–4 times more efficient than direct photon transmission.

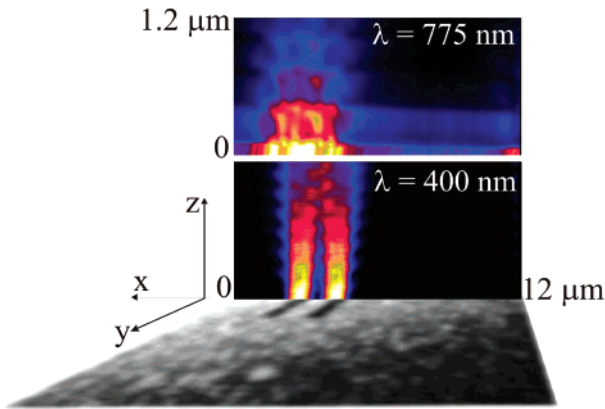


**Figure 3.** Scanning the tip normal to the surface ( $Oz$  direction) in a plane, which contains a line crossing the pair of slits ( $Ox$  direction), reveals the characteristics of the SPP coupling zone. Top panel: 750 nm wavelength, bottom panel: 400 nm, no SPP emission.

The extraordinary transmission enhancement discovered by Ebbesen et al.<sup>24</sup> in metal films perforated by arrays of subwavelength holes is generally believed to be due to the excitation of coupled SPPs on the upper and lower interfaces of the film. However, in our case, the lower interface does not support plasmons due to strong semiconductor absorption. More likely then, when plasmons are present, nonradiative propagation continues efficiently from the horizontal surface down to the semiconductor surface along the slit walls. Because the weighting of the nonradiative modes is greater than the weighting of radiative modes, the energy transfer is more efficient with respect to direct photon excitation. The SPPs reach the other side of the film where they decay into semiconductor excitations without major losses by scattering conversion from plasmons to free photons again, on the rims of the nanoslits. Therefore, the SPP-assisted transmission enhancement can be at least partially explained as resulting from a possible vertical waveguide-mode resonance.<sup>25</sup>

To study in more detail the role of the distribution of the lateral wave-vectors, which couple to the SPP, we continuously varied the gap between the tip and the surface, while continuously scanning laterally in one dimension across a slit pair, Figure 3. SPPs (and therefore photocurrent signal) couple over a distance of 290 nm normal to the surface, for  $\lambda = 775$  nm photons, but are totally absent at  $\lambda = 400$  nm.

The importance of the slit geometrical arrangement is revealed in Figure 4 by choosing mutually orthogonal light polarization directions along the symmetry axes of the pair of slits. The relative intensities as well as the spatial photocurrent pattern are very different for the two polarizations. The light polarization determines the plasmon emission direction. The three slit pairs in the figure are separated by 1.5  $\mu\text{m}$ , 1  $\mu\text{m}$ , and 0.5  $\mu\text{m}$ . When the incident polarization is parallel to the slits, the SPP-generated photocurrent pattern clearly shows that the near-field aperture behaves as a point dipole. The distance between the slit pairs is longer than the horizontal decay length and the slits communicate through SPP waves. When the light polarization is perpendicular to the slit axis, Figure 4a, a “W” pattern emerges. This is

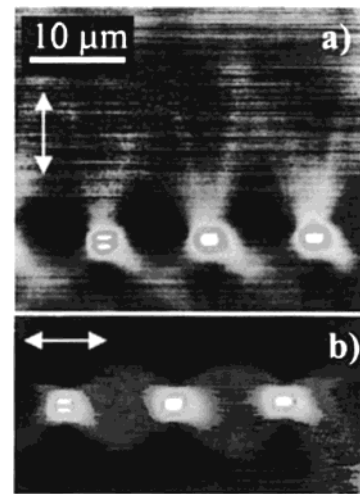


**Figure 4.** Photocurrent images of three parallel slit pairs of different gaps between the slits. From left to right, the gap is 1.5  $\mu\text{m}$ , 1.0  $\mu\text{m}$ , and 0.5  $\mu\text{m}$ . (a) Incident light polarization is perpendicular to the slits, (b) incident light polarization is parallel to the slits. The photocurrent map was taken with the tip at  $\sim 180$  nm from the surface. The intensity map is logarithmic, to emphasize the spatial structure of the surface plasmon coupling between the slit and the near-field tip.

reminiscent of the diffraction pattern calculated by Shchegrov et al. for scattering of surface plasmons on finite-size surface defects.<sup>26</sup> Another explanation for it may be imperfections of the tip and/or slit shape. However, if the tip were the cause, one would have the same “fingers” in Figure 4b, too.

The SPP “fingers” in Figure 4a extend farther for the slit pair having the smallest separation. Decreasing the distance between the slits from 1.5  $\mu\text{m}$  to 0.5  $\mu\text{m}$  seems therefore to increase the SPP coupling with the slit system. We infer from this observation that the SPPs tunnel through the first slit and the entire pair system acts as a Fabry–Perot resonator or a multilayered mirror.

Photocurrent images do not probe directly the plasmon spatial distribution, but rather the overall local efficiency of coupling between the field emitted by the tip and the possible surface electromagnetic states for an area of the order of 100  $\mu\text{m}^2$  compatible with the boundary conditions imposed by the surface structures and the tip position. The lateral spread of wave-vectors available for coupling into plasmons decreases with the gap between the tip and the surface. To point out an interesting implication of this fact, we present here two constant height mode photocurrent images: one at the upper vertical limit of the SPP-coupling zone (200 nm gap, Figure 5c) and the other at a short height from the surface (8 nm gap, Figure 5b). One can readily notice, in the case of the smallest gap, that sharp variations of photocurrent signal are present and correlate well, although not entirely, with the topographic roughness (Figure 5a). The constant height mode has been chosen to minimize possible topographic artifacts. When increasing the gap close to the limit of plasmon coupling, the sharply corrugated photocurrent landscape gives way to a pattern of spatially extended undulations with a period of  $378 \pm 2$  nm (half of the SPP wavelength).

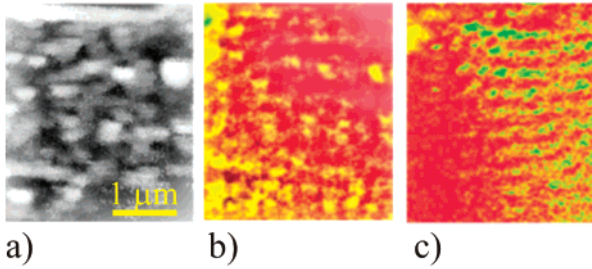


**Figure 5.** Topographic (a) and constant-height (shear-force feedback disabled) photocurrent images at two different gaps between the tip and the surface: (b) 8 nm gap, photocurrent range 125 nA and (c) 200 nm gap, photocurrent range 250 pA. Excitation wavelength 775 nm.

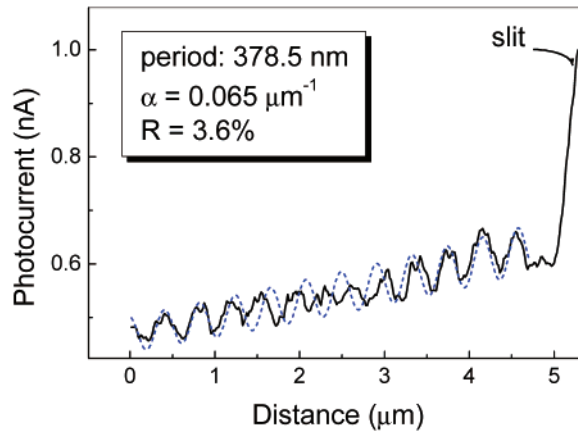


**Figure 6.** Photocurrent intensity vs lateral distance between the tip and the edge of a slit (continuous line) and fitting (dashed line) using a one-dimensional damped wave interference model.

In the case of the 200 nm gap we observe therefore a narrower, quasi-monochromatic spectral distribution of the excited electromagnetic eigenmodes of the surface. The period of the photocurrent pattern in this case corresponds to the interference between delocalized SPPs emitted by the tip, with secondary SPPs reflected from obstacles (slits). From the modulation of the interference pattern, Figure 6, one can estimate the reflection coefficient of a slit.<sup>19</sup> From the overall signal change with the lateral distance between the NSOM aperture and the slit, one can find the SP attenuation length.

In a first approximation, a one-dimensional model based on the interference between a damped planar wave,  $u_+(x,t)$ , and its image reflected by the slit,  $u_-(x,t)$ <sup>27</sup> yields the wave intensity at the slit:

$$|u_+ + u_-|^2 = Ce^{-\alpha x} [1 + 2\rho \cos(2kx - \theta) + \rho^2]$$

where  $C$  is a constant factor including contributions from the SPP wave intensity at excitation, the transmission efficiency through the slit, and the conversion of SPPs into excited electron–hole pairs,  $x$  is the distance between the tip and the slit,  $\alpha$  is the attenuation coefficient,  $\rho^2 = R$  is the reflection coefficient, and  $\theta$  is the phase shift at reflection.

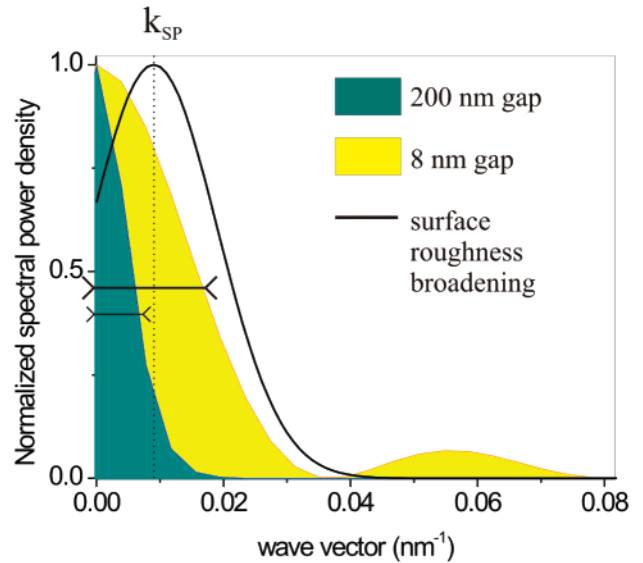


**Figure 7.** Schematic of the SPP coupling that occurs when the  $k$ -vector distribution of the impinging radiation overlaps with the roughness-broadened  $k$ -vector distribution of the SPP. A quasi-monochromatic selection of electromagnetic plasmon modes is possible only when the edges of the two distributions barely overlap (200 nm gap). The  $k$ -vector distributions in the near-field were calculated using the Bethe–Bouwkamp model.

A 3.6% reflection coefficient and a  $0.065 \mu\text{m}^{-1}$  linear attenuation coefficient are obtained as fit parameters for the experimental intensity vs distance variation, Figure 6. When the tip is close to the surface, electromagnetic radiation from the aperture impinging on the surface has a broad spectrum of spatial frequencies, with a cutoff at approximately  $2\pi/a$ , where  $a$  is the diameter of the tip aperture,<sup>28</sup> Figure 7. The physical process causing the spatial frequency fluctuations necessary to reconstruct the surface roughness in a photocurrent image is the scattering of near-field photon wavevectors on surface spatial perturbations, which effectively broadens the SPP spectrum. In order for plasmons to be emitted, overlap between the tip-limited photon  $k$ -vector spectrum and surface-roughness-limited plasmon  $k$ -vector spectrum must occur. The result of a complete overlapping is a broad spectrum of SPP spatial frequencies, allowing for the sharp, localized features in Figure 5b. In the case of limited overlap between the SPP spectrum and the photon spectrum, occurring at the 200 nm gap, a narrower bandwidth for plasmon spatial frequencies is achieved, Figure 7. One obtains therefore a coherent, quasi-monochromatic surface plasmon emission, similar to the one obtained on smooth surfaces. Note that, in this case, significantly lower photocurrent intensity occurs than for short gaps. It is worthwhile to point out that the exact shape of the wings of the tip spatial frequency distribution and the surface spatial frequency distribution will determine the behavior, as seen from Figure 7.

In conclusion, the possibility of switching between localized and delocalized electromagnetic mode excitation by using the tip/surface gap variable is a distinctive and potentially useful feature of the near-field coupling scheme. Our results show that surface plasmon coherence can be

maintained even over rough surfaces when appropriate coupling conditions are reached. In addition, our findings support the proposed picture of plasmons propagating along the inner walls of deep holes in optically thick gold films.

**Acknowledgment.** The authors gratefully acknowledge financial support by the National Institute of Standards and Technology and by the National Science Foundation. B.D. thanks William Schaich for many discussions.

## References

- (1) Raether, H. *Surface Plasmons on Smooth and Rough Surfaces and on Gratings*; Springer-Verlag: Berlin, 1988.
- (2) Moskovits, M. *Rev. Mod. Phys.* **1985**, *57*, 783.
- (3) Chance, R. R.; Prock, A.; Silbey, R. In *Advanced Chemical Physics*; Prigogine, I., Rice, S. A., Eds.; Wiley: New York, 1978; vol. XXXVII, p 1.
- (4) Weber, W. H. Eagen, C. F. *Opt. Lett.* **1979**, *4*, 236.
- (5) Lushnikov, A. A.; Maksimenko, V. V.; Simonov, A. J. In *Electromagnetic Surface Modes*; Boardman, A. D., Ed.; John Wiley & Sons: New York, 1982; p 305.
- (6) Ebbesen, T. W.; Lezec, H. J.; Ghaemi, H. F.; Thio, T.; Wolff, P. A. *Nature* **1998**, *391*, 667.
- (7) Sanchez-Gil, J. A.; Maradudin, A. A. *Phys. Rev. B* **1999**, *60*, 8359.
- (8) Bohn, P. W. *Annu. Rev. Mater. Sci.* **1997**, *27*, 469.
- (9) Yokota, H.; Saito, K.; Yanagida, T. *Phys. Rev. Lett.* **1998**, *80*, 4606.
- (10) Tsvetkov, A. A.; van der Marel, D.; Moler, K. A.; Kirtley, J. R.; de Boer, J. L.; Meetsma, A.; Ren, Z. F.; Kolesnikov, N.; Dulic, D.; Damascelli, A.; Grüninger, M.; Schützmann, J.; van der Eb, J. W.; Somal, H. S.; Wang, J. H. *Nature* **1998**, *395*, 360.
- (11) Collier, C. P.; Vossmeier, T.; Heath, J. R. *Annu. Rev. Phys. Chem.* **1998**, *49*, 371.
- (12) Dick, L. A.; McFarland, A. D.; Haynes, C. L.; Van Duyne, R. P. *J. Phys. Chem. B* **2002**, *106*, 853.
- (13) Specht, M.; Pedarnig, J. D.; Heckl, W. M.; Hänsch, T. W. *Phys. Rev. Lett.* **1992**, *68*, 476.
- (14) Hecht, B.; Bielefeldt, H.; Novotny, L.; Inouye, Y.; Pohl, D. W. *Phys. Rev. Lett.* **1996**, *77*, 1889.
- (15) Bozhevolnyi, S. I.; Pudonin, F. A. *Phys. Rev. Lett.* **1997**, *78*, 2823.
- (16) Pohl, D. W. *Top. Appl. Phys.* **2001**, *81*, 1.
- (17) Chicanne, C.; David, T.; Quidant, R.; Weeber, J. C.; Lacroute, Y.; Bourillot, E.; Dereux, A. *Phys. Rev. Lett.* **2002**, *88*, art. no. 097402.
- (18) des Francs, G. C.; Girard, C.; Weeber, J. C.; Chicane, C.; David, T.; Dereux, A.; Peyrade, D. *Phys. Rev. Lett.* **2001**, *86*, 4950.
- (19) Bouhelier, A.; Huser, Th.; Tamaru, H.; Güntherodt, H.-J.; Pohl, D. W. *Phys. Rev. B* **2001**, *63*, 155404.
- (20) Sönnichsen, C.; Duch, A. C.; Steininger, G.; Koch, M.; von Plessen, G.; Feldmann, J. *Appl. Phys. Lett.* **2000**, *76*, 140.
- (21) Khosravi, H.; Tilley, D. R.; Loudon, R. *J. Opt. Soc. Am. A* **1991**, *8*, 112.
- (22) Novotny, L.; Hafner, C. *Phys. Rev. E* **1994**, *50*, 4094.
- (23) Bouwkamp, C. J. *Philips Res. Rep.* **1950**, *5*, 321.
- (24) Ebbesen, T. W.; Lezec, H. J.; Ghaemi, H. F.; Thio, T.; Wolf, P. A. *Nature* **1998**, *391*, 667.
- (25) Cao, Q.; Lalanne, P. *Phys. Rev. Lett.* **2002**, *88*, 057403.
- (26) Shchegrov, A. V.; Novikov, I. V.; Maradudin, A. A. *Phys. Rev. Lett.* **1997**, *78*, 4269.
- (27) Morse, P. M.; Feshbach, H. *Methods of Theoretical Physics, Part I*; McGraw-Hill: Boston, 1953.
- (28) Fillard, J. P. *Near Field Optics and Nanoscopy*; World Scientific: Singapore, 1996.

NL020207L